A Maximum A Posteriori Approach of Hyperanalytic Wavelet Based Image Denoising in a Multi-Wavelet Context

Ioana Firoiu[1,2], Alexandru Isar[1] and Dorina Isar[1]
1-"Politehnica" University, Electronics and Communications Faculty, Timisoara, Romania,
2-Telecom Bretagne, Brest, France
E-mail, ioana.firoiu@etc.upt.ro, dorina.isar@etc.upt.ro, alexandru.isar@etc.upt.ro

***Abstract*- In this paper we propose the use of a new implementation of the hyperanalytic wavelet transform, (HWT), in association with a Maximum a Posteriori (MAP) filter named bishrink. Such a denoising method is sensitive to the selection of the mother wavelets used for the computation of the HWT. Taking into account the drawbacks of the bishrink filter and the sensibility with the selection of the mother wavelets we propose a denoising method in two stages in a multi-wavelet context. Some simulation examples and comparisons prove the performances of the proposed denoising method.**

I. INTRODUCTION

Images are often corrupted by additive noise that can be modeled as Gaussian most of the time [5-12], [14,15]. David Donoho introduced the word denoising in association with the wavelet theory, [1]. The corresponding denoising method has three steps, [1]: 1) the computation of the forward wavelet transform (WT), 2) the filtering of the wavelet coefficients, 3) the computation of the inverse WT (IWT) of the result obtained.

Numerous WTs can be used to operate these treatments. The first one was the Discrete Wavelet Transform, DWT, [1]. It has three main disadvantages, [2]: lack of shift invariance, lack of symmetry of the mother wavelets and poor directional selectivity. These disadvantages can be diminished using a complex wavelet transform [2, 3]. In the present paper we propose the use of a very simple implementation of the HWT, recently proposed, [4]. It has a high shift-invariance degree versus other quasi-shift-invariant WTs with the same redundancy. It has also an enhanced directional selectivity. All the WTs have two parameters: the mother wavelets, MW and the primary resolution, PR, (number of iterations). The importance of their selection is highlighted in [5]. Another appealing particularity of those transforms is the interscale dependency of the wavelet coefficients.

Numerous non-linear filter types can be used in the WT domain. First, non-parametric filters were used: the hard-thresholding filter, [1], the soft-thresholding filter, [1, 6], that minimizes the Min-Max estimation error and the Efficient SURE-Based Inter-scales Pointwise Thresholding filter [7], which minimizes the Mean Square Error, (MSE). Next were constructed filters obtained by minimizing a Bayesian risk under a cost function, typically a delta cost function (maximum a posteriori (MAP) estimation [8-10]) or the minimum mean squared error (MMSE) estimation [11]. The construction of MAP filters supposes the existence of two statistical models, for the useful component of the input image and for its noise component. The MAP estimation of w, realized using the observation $y=w+n$, (where n represents the WT of the noise n_i and w the WT of the useful component of the input image s, $f=s+n_i$) is given by the following relation, called MAP filter equation:

$$\hat{w}(y) = \arg\max_{w}\left\{ln\left(f_n(y-w)\,f_w(w)\right)\right\} \qquad (1)$$

where f_α represents the probability density function (pdf) of α.

Generally, the noise component is assumed Gaussian distributed. For the useful component there are many models: the family of Pearson's distributions [8], the Laplace distribution [9], the family of SαS distributions [10], or the Gauss-Markov random field model [12]. This distribution changes from scale to scale. For the first iterations of the WT it is a heavy tailed distribution. There are two solutions to deal with this mobility. The first one assumes the use a simple fixed model, risking a decrease in accuracy across the scales. This is the case of the bishrink filter [9]. The second solution assumes to use a generalized model, defining a family of distributions and the identification of the best fitting element of this family for the distribution of the wavelet coefficients at a given scale [8, 10, 12]. The use of such generalized models makes the treatment more accurate but requires more sophisticated parameter identification strategies. If the pdfs f_w and f_n do not take into account the interscale dependency of the wavelet coefficients than the MAP filter obtained is called marginal. This paper proposes a new denoising method adapted to the multi-wavelet context. The proposed method supposes the multiple use of a very simple generic denoising method that implies three steps: the computation of the forward HWT using the new implementation [4], the filtering in the wavelets domain with the aid of the bishrink filter [9] and the computation of the inverse HWT, (IHWT). Each application of the generic denoising method utilizes different mother wavelets and produces a different partial result. Next, the final result is synthesized from the partial results. The second section resumes the new implementation of the HWT. The third section presents the bishrink filter. The aim of the

fourth section is the partial results synthesis mechanism. The paper concludes with few final remarks.

II. HWT

The generalization of the analyticity concept in 2D is not obvious, because there are multiple definitions of the Hilbert transform in this case. In the following we will use the definition of the analytic signal associated to a 2D real signal named hypercomplex signal.

A. Implementation

The hypercomplex mother wavelet associated to the real mother wavelet $\psi(x,y)$ is defined as:

$$\begin{aligned}\psi_a(x,y) &= \psi(x,y) + i\mathcal{H}_x\{\psi(x,y)\} + \\ &+ j\mathcal{H}_y\{\psi(x,y)\} + k\mathcal{H}_x\{\mathcal{H}_y\{\psi(x,y)\}\}\end{aligned} \tag{2}$$

where $i^2 = j^2 = -k^2 = -1$, *and* $ij = ji = k$, [13].

The HWT of the image $f(x,y)$ is:

$$HWT\{f(x,y)\} = \langle f(x,y), \psi_a(x,y)\rangle. \tag{3}$$

Taking into account relation (2) it can be written:

$$\begin{aligned}&HWT\{f(x,y)\} = DWT\{f(x,y)\} + \\ &iDWT\{\mathcal{H}_x\{f(x,y)\}\} + jDWT\{\mathcal{H}_y\{f(x,y)\}\} + \\ &+kDWT\{\mathcal{H}_y\{\mathcal{H}_x\{f(x,y)\}\}\} = \\ &\langle f_a(x,y), \psi(x,y)\rangle = DWT\{f_a(x,y)\},\end{aligned} \tag{4}$$

where the index *a* specify the fact that the associated function is hypercomplex. Consequently, the 2D-HWT of the image $f(x,y)$ can be computed with the aid of the 2D-DWT of its associated hypercomplex image. The new HWT implementation, [4], presented in figure 1, uses four trees, each one implementing a 2D-DWT. The first tree is applied to the input image. The second and the third trees are applied to 1D discrete Hilbert transforms computed across the lines ($\mathcal{H}_x$) or columns ($\mathcal{H}_y$) of the input image. The fourth tree is applied to the result obtained after the computation of the two 1D discrete Hilbert transforms of the input image. These are the so called initial computations. To obtain an enhanced directional selectivity some additional linear operations, represented in the right part of figure 1, must be performed [4]. The result is composed by two sequences of complex coefficients:

$$z_+ = z_{+r} + jz_{+i} = (d_1 - d_4) + j(d_2 + d_3) \tag{5}$$

containing three subbands with positive angle direction orientations $\text{atan}(1/2)$, $\pi/4$ and $\text{atan}(2)$ and:

$$z_- = z_{-r} + jz_{-i} = (d_1 + d_4) + j(d_2 - d_3) \tag{6}$$

containing three subbands with negative angle direction orientations $-\text{atan}(1/2)$, $-\pi/4$ and $-\text{atan}(2)$.

The main advantage of the proposed implementation of HWT is that this complex transform is reduced to the computation of the 2D DWT, permitting the heritage of some classes of mother wavelets, like the Daubechies, Symmlet or Coiflet families. This is why this implementation is adequate to a multi-wavelet environment.

B. Second order statistical analysis

We begin by making the second order statistical analysis of the 2D DWT. The lines of the input image (obtained at the end of the previous iteration) are passed trough two different filters (a lowpass filter having the impulse response m_0 and a

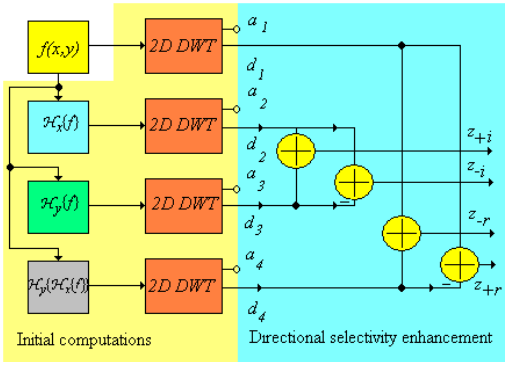

Figure 1. The new HWT-implementation architecture.

high-pass filter m_1) resulting two different sub-images. Then the lines of the two images are decimated with a factor of 2. Next, the columns of the two images obtained are low-pass filtered with m_0 and high-pass filtered with m_1. The columns of those four images are also decimated with a factor of 2. Four new images (representing the result of the current iteration) are obtained. The first sub-image, obtained after two lowpass filtering, is named approximation image (or LL image). The other three are named detail sub-images: LH, HL and HH. The LL sub-image represents the input for the next iteration. In the following, the coefficients of the DWT will be denoted with ${}_fD_m^k$, where f represents the image who's DWT is computed, m represents the iteration index and k = 1, for the HH image, k = 2, for the HL image, k = 3, for the LH image and k = 4, for the LL image. These coefficients are computed using the following relation:

$${}_xD_m^k[n_1,p_1] = \langle x(\tau_1,\tau_2), \psi_{m,n_1,p_1}^k(\tau_1,\tau_2)\rangle, \tag{7}$$

where the wavelets can be factorized:

$$\psi_{m,n,p}^k(\tau_1,\tau_2) = \alpha_{m,n}^k(\tau_1)\cdot\beta_{m,p}^k(\tau_2), \tag{8}$$

and the two factors can be computed using the scale function $\varphi(\tau)$ and the mother wavelets $\psi(\tau)$:

$$\alpha_{m,n}^k(\tau) = \begin{cases}\varphi_{m,n}(\tau), & k = 1,\ 4\\ \psi_{m,n}(\tau), & k = 2,\ 3\end{cases}, \tag{9}$$

$$\beta_{m,p}^k(\tau) = \begin{cases}\varphi_{m,p}(\tau), & k = 2,\ 4\\ \psi_{m,p}(\tau), & k = 1,\ 3\end{cases}, \tag{10}$$

where:

$$\begin{aligned}&\varphi_{m,n}(\tau) = 2^{-\frac{m}{2}}\varphi\left(2^{-m}\tau - n\right) \text{ and}\\ &\psi_{m,n}(\tau) = 2^{-\frac{m}{2}}\psi\left(2^{-m}\tau - n\right).\end{aligned} \tag{11}$$

Taking into account equations (9)-(11) it can be written:

$$\psi^k_{m,n,p}(\tau_1,\tau_2) = 2^{-m}\psi^k\left(2^{-m}\tau_1 - n, 2^{-m}\tau_2 - p\right), \quad (12)$$

where $\psi^k(\tau_1,\tau_2) = \psi^k{}_{0,0,0}(\tau_1,\tau_2)$.

The correlation function of the wavelet coefficients can be computed using the following relation:

$$\Gamma_{{}_f D^k_m}[n_1,n_2,p_1,p_2] = \\ = \frac{1}{4\pi^2}\int_{R^2}\gamma_f\left(2^{-m}\nu_1, 2^{-m}\nu_2\right)\cdot\left|\mathcal{F}\left\{\psi^k(\nu_1,\nu_2)\right\}\right|^2 \cdot \\ \cdot e^{j\left[\nu_1(n_2-n_1)+\nu_2(p_2-p_1)\right]}d\nu_1 d\nu_2 \quad (13)$$

where γ_f represents the power spectral density of the input image f while the square of the absolute value representing the second factor in the integral from the right hand side of the last equation is the power spectral density of the mother wavelets which generates the subband k.

If the input image consists of a white Gaussian noise, with a known variance, σ_n^2, then:

$$\Gamma_{{}_{n_i} D^k_m}[n_1,p_1] = \sigma_n^2\cdot\delta[n_1]\cdot\delta[p_1]. \quad (14)$$

So, the 2D-DWT does not correlate the white Gaussian noise, all the detail coefficient sequences are zero mean white noises with the same variance equal with the variance of the input signal σ_n^2. The same result can be obtained taking in (13) the limit for $m\to\infty$. So, asymptotically the 2D DWT transforms every colored noise into a white one. Hence this transform can be regarded as a whitening system. Finally, the correlation of the 2D-DWT of s is given by:

$$\Gamma_{{}_s D^k_m}[n_1,p_1] = 2^{2m}\cdot\Gamma_s\left[2^m n_1, 2^m p_1\right], \quad (15)$$

We continue with the second order statistical analysis of the HWT detail coefficients. The imaginary part of the coefficients z_+ are computed using the following relation:

$$ {}^{+i}_{f}z^k_m[n_1,p_1] = {}^{2}_{f}D^k_m[n_1,p_1] + {}^{3}_{f}D^k_m[n_1,p_1] = \\ = \left\langle \mathcal{H}_x\{f\}(\tau_1,\tau_2) + \mathcal{H}_y\{f\}(\tau_1,\tau_2), \psi^k_{m,n_1,p_1}(\tau_1,\tau_2)\right\rangle$$

Their correlation function can be computed using the following relation:

$$\Gamma_{{}^{+i}_{f}z^k_m}[n_1,n_2,p_1,p_2] = E\left\{ {}^{+i}_{f}z^k_m[n_1,p_1]\left({}^{+i}_{f}z^k_m[n_2,p_2]\right)^*\right\} = \ldots$$

Each term of the right hand side $T_l, l=1,\ldots,4$ can be written in the form given in (13) because it is the result of a 2D DWT. In consequence:

$$\Gamma_{{}^{+i}_{f}z^k_m}[n_1,n_2,p_1,p_2] = \frac{1}{4\pi^2}\int_{R^2}\Big(\gamma_{\mathcal{H}_x\{f\}} + \gamma_{\mathcal{H}_x\{f\}\mathcal{H}_y\{f\}} \\ +\gamma_{\mathcal{H}_y\{f\}\mathcal{H}_x\{f\}} + \gamma_{\mathcal{H}_y\{f\}}\Big)\left(2^{-m}\nu_1, 2^{-m}\nu_2\right)\cdot \\ \cdot\left|\mathcal{F}\left\{\psi^k(\nu_1,\nu_2)\right\}\right|^2\cdot e^{j\left[\nu_1(n_2-n_1)+\nu_2(p_2-p_1)\right]}d\nu_1 d\nu_2$$

which can be put in the following form:

$$\Gamma_{{}^{+i}_{f}z^k_m}[n_1,n_2,p_1,p_2] = \frac{1}{4\pi^2}\cdot \\ \cdot\int_{R^2}\Big[\left(|sgn\,\xi_1|^2 + 2\,sgn\,\xi_1\,sgn\,\xi_2 + |sgn\,\xi_2|^2\right) \\ \left(\xi_1 = 2^{-m}\nu_1, \xi_2 = 2^{-m}\nu_2\right)\cdot\left|\mathcal{F}\left\{\psi^k(\nu_1,\nu_2)\right\}\right|^2\cdot \\ \cdot e^{j\left[\nu_1(n_2-n_1)+\nu_2(p_2-p_1)\right]}d\nu_1 d\nu_2 \quad (16)$$

The asymptotic behavior of the coefficients z_{+i} can be obtained if the limit for $m\to\infty$ is taken into the last relation:

$$\Gamma_{{}^{+i}_{f}z^k_\infty}[n_1,n_2,p_1,p_2] = 0, \quad (17)$$

because $sgn\,0 = 0$. Similar considerations can be made for the other coefficients, z_{+r}, z_{-i} and z_{-r}. Hence, asymptotically the detail coefficients of the HWT are decorrelated. Further consideration can be made following the same line of reasoning on the first two moments of the coefficients z and on the case when the input image is a White Gaussian Noise (WGN). So, the HWT has a statistical comportment similar to that of the 2D DWT but has better translation invariance and directional selectivity [4]. As a result, the real and the imaginary parts of the HWT detail coefficients of the noise n_i represent white noise sequences. It can be proved that these sequences are also Gaussians.

C. Mother Wavelets Time-Frequency Localization

A measure of the time-frequency localization of a given signal can be obtained by the product between the squared values of the effective signal duration, σ_t^2 and of its effective bandwidth, σ_ω^2. For a certain signal, $x(t)$, the two are defined as:

$$\sigma_t^2 = \frac{\int_{-\infty}^{\infty} t^2|x(t)|^2\,dt}{\int_{-\infty}^{\infty}|x(t)|^2\,dt} \text{ and } \sigma_\omega^2 = \frac{\int_{-\infty}^{\infty}\omega^2|X(\omega)|^2\,d\omega}{\int_{-\infty}^{\infty}|X(\omega)|^2\,d\omega}.$$

According to Heisenberg's incertitude criterion, applied in the signal processing context, this product is higher than $\pi/2$. In [14] were estimated the time-frequency localizations of the elements of the Daubechies mother wavelets family and was proved that the time-frequency localization of those elements monotonically increases with the number of vanishing moments. The time variable of the one dimensional signals is replaced with a space variable in the case of images. So, the effective duration of a one dimensional signal can be replaced with an effective spatial spreading of an image. In consequence the space-frequency localization could be an important criterion for the segmentation of images.

III. THE BISHRINK FILTER

The Bishrink Filter is a MAP filter that takes into account the interscale dependency of the wavelet coefficients considering the bivariate pdfs, $f_{\mathbf{n}}$ and $f_{\mathbf{w}}$ in (1).

A. Construction

As a consequence of the conclusion of the previous paragraph, the noise is assumed i.i.d. Gaussian,

$$f_{\mathbf{n}}(\mathbf{n}) = \frac{1}{2\pi\sigma_n^2} \cdot e^{-\frac{n_1^2+n_2^2}{2\sigma_n^2}}. \quad (18)$$

The model of the noise-free image is given by:

$$f_{\mathbf{w}}(\mathbf{w}) = \frac{3}{2\pi\sigma^2} \cdot e^{-\frac{\sqrt{3}}{\sigma}\sqrt{w_1^2+w_2^2}}, \quad (19)$$

a heavy tailed distribution. Substituting these two pdfs in the equation of the MAP filter (1) and solving it, the following solution is obtained:

$$\hat{w}_1 = \frac{\left(\sqrt{y_1^2+y_2^2} - \frac{\sqrt{3}\sigma_n^2}{\sigma}\right)_+}{\sqrt{y_1^2+y_2^2}} y_1. \quad (20)$$

where:

$$(X)_+ = \begin{cases} X, & \text{for} \quad X > 0 \\ 0, & \text{otherwise} \end{cases}.$$

We can observe that the bishrink filter has a dead zone. This estimator requires prior knowledge of the noise variance and of the marginal variance of the noise-free image for each wavelet coefficient. To estimate the noise variance from the noisy wavelet coefficients, a robust median estimator from the finest scale wavelet coefficients obtained by applying the 2D DWT is used [1]:

$$\hat{\sigma}_n^2 = \frac{\text{median}\left(|y_i|\right)}{0.6745}, \quad y_i \in \text{subband HH}. \quad (21)$$

In [9] the marginal variance of the k^{th} coefficient is estimated using neighboring coefficients in the region $N(k)$, a squared shaped window centered on this coefficient with size 7×7. To make this estimation one gets $\sigma_y^2 = \sigma^2 + \sigma_n^2$ where σ_y^2 represents the marginal variance of noisy observations y_1 and y_2. For the estimation of the marginal variance of noisy observations, in [9] is proposed the following relation:

$$\hat{\sigma}_y^2 = \frac{1}{M} \sum_{y_i \in N(k)} y_i^2, \quad (22)$$

where M is the size of the neighborhood $N(k)$. Then σ can be estimated as:

$$\hat{\sigma} = \sqrt{\left(\hat{\sigma}_y^2 - \hat{\sigma}_n^2\right)_+} \quad (23)$$

For the estimation of the local standard deviation of the useful component of the parent coefficients $\hat{\sigma}_2$ in a given subband, first the subband is interpolated by repeating each line and column. Second the relations (22) and (23) are applied.

Tacking into account the simplicity of its statistical model (which permits to find an analytical solution of the MAP filter equation (1)) based only on two parameters ($\hat{\sigma}$ and $\hat{\sigma}_n$ which can be easily identified using the relations (21), (22) and (23)) and its performance (reported in [9]), the bishrink can be considered as one of the best filters that can be applied in the wavelet domain. It can be associated with different WTs, 2D DWT, Double Tree Complex Wavelet Transform (DTCWT) [3] or HWT. In the case of the association with complex WTs, there are two ways of applying the bishrink filter, separately to the real and imaginary parts of the detail coefficients or to the magnitudes of those coefficients. The second solution has better performance because in this case the corresponding complex WT is less translation sensitive.

B. Drawbacks

The sensitivity of the bishrink filter with the estimation of the noise standard deviation $\hat{\sigma}_n$ is:

$$S_{\hat{w}_1}^{\hat{\sigma}_n} = \frac{d\hat{w}_1}{d\hat{\sigma}_n} \cdot \frac{\hat{\sigma}_n}{\hat{w}_1},$$

Taking into account its input-output relation, we obtain:

$$S_{\hat{w}_1}^{\hat{\sigma}_n} = \begin{cases} \frac{-2\sqrt{3}\hat{\sigma}_n^2}{\hat{\sigma}\sqrt{y_1^2+y_2^2} - \sqrt{3}\hat{\sigma}_n^2}, & \text{if } \sqrt{y_1^2+y_2^2} > \frac{\sqrt{3}\hat{\sigma}_n^2}{\hat{\sigma}} \\ 0, & \text{otherwise} \end{cases}. \quad (24)$$

The absolute value of this sensitivity is an increasing function of $\hat{\sigma}_n$. When the value of the estimation of the noise standard deviation is higher then the performance of the bishrink filter is poorer. Another very important parameter of the bishrink filter is the local estimation of the marginal variance of the noise-free image $\hat{\sigma}$. The sensitivity of the estimation $\hat{w}_1$ with $\hat{\sigma}$ is given by:

$$S_{\hat{w}_1}^{\hat{\sigma}} = \begin{cases} \frac{\sqrt{3}\hat{\sigma}_n^2}{\hat{\sigma}\sqrt{y_1^2+y_2^2} - \sqrt{3}\hat{\sigma}_n^2}, & \text{if } \sqrt{y_1^2+y_2^2} > \frac{\sqrt{3}\hat{\sigma}_n^2}{\hat{\sigma}} \\ 0, & \text{otherwise} \end{cases}. \quad (25)$$

This is a decreasing function of $\hat{\sigma}$. The precision of the estimation based on the use of the bishrink filter decreases with the decreasing of $\hat{\sigma}$.

The local variance of a pixel $\hat{\sigma}$ can be interpreted in two ways. First it represents a homogeneity degree measure for the region to which the considered pixel belongs. The regions with high homogeneity correspond to the dark regions in the image of local variances. All the pixels belonging to a perfect homogeneous region have the same value. So, their local variances are equal to zero. The values of the pixels belonging to a textured region oscillate in space and they have not null local variances. Finally, the pixels belonging to an edge have the higher local variances. **We can observe that the bishrink filter treats the edges very well, the estimation of the textured regions must be corrected and the worst treatment corresponds to the homogeneous regions.** The denoising quality of pixels with slightly different σ will be very different in the homogeneous regions. The sensitivity $S_{\hat{w}_1}^{\hat{\sigma}}$ increases with the increasing of $\hat{\sigma}_n$. So, the degradation of the homogeneous and textured zones of the noise-free image is amplified by the increasing of the noise standard deviation. **Consequently the most difficult regime of the bishrink filter corresponds to the treatment of homogeneous regions of very noisy images.** Secondly, the local variance of a pixel gives some information about the frequency content of the region to which the considered pixel belongs. If the pixels of a given region have low local variances then the considered region contains low

frequencies. If these pixels have high local variances then the considered region contains high frequencies. The denoising method based on the use of the bishrink filter is also sensitive to the mother wavelets selection. For example in the following table are presented the values of the output peak signal to noise ratios (PSNR) obtained using the association of the bishrink filter with different HWTs (computed using

TABLE I
OUTPUT PSNRS OBTAINED DENOISING THE IMAGE LENA PERTURBED WITH AWGN WITH DIFFERENT STANDARD DEVIATIONS (FIRST COLUMN) USING HWTS COMPUTED WITH THE AID OF THE FIRST SEVEN MOTHER WAVELETS FROM THE DAUBECHIES FAMILY (THE FOLLOWING COLUMNS)

σ_n	1	2	3	4	5	6	7
10	34.1	34.1	34.2	34.3	**34.3**	**34.3**	34.3
15	32.2	32.2	32.3	32.4	**32.5**	32.4	32.4
20	30.8	30.8	30.9	31.0	31.0	31	31
25	29.8	29.9	30	30.1	**30.1**	30.1	30.1
30	29	29	29.1	29.3	**29.2**	29.2	29.1
35	28.29	28.34	28.46	28.59	**28.61**	28.51	28.45

the mother wavelets from the Daubechies family) for the denoising of the image Lena perturbed with Additive WGN (AWGN). The bishrink was applied to the magnitudes of the HWT detail coefficients and for the estimation of σ were used rectangular windows. So the performance of the denoising method based on the association of the HWT with the bishrink filter is different for different mother wavelets. In consequence, the performance could be improved in a multi-wavelet context.

IV. PROPOSED METHOD

Tacking into consideration the idea in section II *C* it can be affirmed that the regions with the best space-frequency localization of the noise-free image must be treated with a HWT computed using the mother wavelets Dau_4 (with 2 vanishing moments) and the regions with the poor space-frequency localization must be treated with a HWT computed using the mother wavelets Dau_20 (with 10 vanishing moments). In consequence a segmentation of the noise-free image made using as criterion the space-frequency localization could help the denoising. The values of the local variances could be used as a measure of space-frequency localization because, as already said in section III *B*, the local variance of a pixel gives some information about the frequency content of the region to which the considered pixel belongs. If the pixels of a given region have low local variances then the considered region contains low frequencies. If these pixels have high local variances then the considered region contains high frequencies. On the other hand, it can be observed that the regions corresponding to pixels with high values of the local variance have good spatial localization and the regions corresponding to pixels with small values of the local variance have poor spatial localization. In consequence we propose a denoising strategy in two steps. In the first step we denoise the input image using the association bishrink filter – HWT (computed with intermediate mother wavelets, for example Dau_12 (with 6 vanishing moments)). Computing the local variances of each pixel of the resulted image we obtain a reference image, I_r. This image is segmented in 9 regions, the pixels of the k^{th} region having the values belonging to the interval $I_k = \left(\varepsilon_{k-1} \cdot \max\{I_r\}, \varepsilon_k \cdot \max\{I_r\}\right),\ k = 1, 2, ..., 9,$ where $\varepsilon_0=0$, $\varepsilon_1=0.15$, $\varepsilon_2=0.225$, $\varepsilon_3=0.25$, $\varepsilon_4=0.3$, $\varepsilon_5=0.6$, $\varepsilon_6=0.7$, $\varepsilon_7=0.8$, $\varepsilon_8=0.9$ and $\varepsilon_9=1$. Collecting the coordinates of the pixels from each region, 9 corresponding binary masks, M_1, M_2,…,M_9 are generated. The second stage of the proposed denoising method consists in the application of the association bishrink filter – HWT (computed using the mother wavelets Dau_2*l*) for each *l*=2, 3, …, 10, to the noisy image. Nine partial results are obtained, PR_1, PR_2, …, PR_9. They are synthesized using a mechanism developed in [14]. To reduce the sensitivity of the bishrink filter with σ, some linear combinations of those partial results are computed, obtaining the new partial results:

$$NPR_1 = PR_1,\ NPR_2 = PR_2, NPR_3 = PR_3, NPR_4 = PR_4, NPR_5 = PR_5,$$
$$NPR_6 = \left(PR_1 + PR_2 + PR_3\right)/3,\ NPR_7 = \left(PR_1 + PR_2 + PR_3 + PR_4\right)/4,$$
$$NPR_8 = \left(PR_1 + PR_2 + PR_3 + PR_4 + PR_5 + PR_6 + PR_7 + PR_8\right)/8,$$
$$NPR_9 = \left(PR_1 + PR_2 + PR_3 + PR_4 + PR_5 + PR_6 + PR_7 + PR_8 + PR_9\right)/9.$$

Each one is multiplied with a different mask obtaining 9 regions:

$$R_k = NPR_k \cdot M_{9-k}\ . \tag{26}$$

The final result is obtained by concatenation.

V. SIMULATION RESULTS

The performance of the denoising systems in [7-16] is appreciated in these references only on the basis of the enhancement of the peak signal to noise ratios (PSNR) produced. This metric is equivalent with other metrics like the Mean Square Error (MSE) or Root MSE (RMSE) because:

$$PSNR = 10 \cdot \lg\left(255^2 / MSE\right) = 20 \cdot \lg\left(255 / RMSE\right).$$

The values of the output PSNRs obtained using the new denoising method for the treatment of the image Lena perturbed with AWGN with different variances are presented in the following table. The bishrink was applied to the magnitudes of the HWT detail coefficients and for the estimation of σ, elliptical windows with principal axis parallel with the preferential direction of the corresponding subband were used this time [15]. The performance of the new denoising method is compared to the performance of similar denoising method [15-18]. The method in [16] has also two stages. In each one the denoising is realized with Wiener filters applied in the 2D DWT domain. In [17] is used the contourlet transform. The denoising methods in both references [16, 17] use directional windows. In [18] is proposed a denoising method which uses the HWT associated with another non-linear filter. Finally, in [15] are proposed some denoising algorithms based on the association of the HWT with a simpler MAP filter. The best results obtained in [15] are presented on the last column of table II.

TABLE II
OUTPUT PSNRS OBTAINED DENOISING THE IMAGE LENA PERTURBED WITH AWGN WITH DIFFERENT STANDARD DEVIATIONS (FIRST COLUMN) USING THE PROPOSED DENOISING METHOD AND THE BEST METHOD IN [15].

σ_n	Noisy	[16]	[17]	[18]	Prop	[15]
10	28.18	34.7	-	-	**34.85**	34.54
20	22.16	31.5	-	31.58	**31.78**	31.42
25	20.20	30.4	-	-	**30.74**	30.37
30	18.62	-	28.77	-	**29.98**	*29.45*
35	17.29	-	-	-	**29.3**	*28.65*
40	16.53	-	27.47	27.74	**28.63**	*27.93*
50	14.18	-	26.46	-	**27.03**	*26.63*

The results obtained applying the denoising method proposed in this paper are the best results in table II. In the following figure is presented the acquired image (σ_n=25) and the result obtained applying the proposed denoising method (bottom). The case of the image Barbara is presented in figure 3. We can remark the good treatment of contours and textures done by the proposed denoising method.

Figure 2. Acquired image (left) and the result of the proposed denoising method (right).

Figure 3. Acquired image (σ_n=25, $PSNR_i$=20.2 dB) (left) and the result of the proposed denoising method ($PSNR_o$=27.7 dB) (right).

VI. Conclusion

In this paper is used a simple implementation of the HWT, which permits the exploitation of the results previously obtained in the wavelets theory. This implementation has a very flexible structure, as we can use any orthogonal or bi-orthogonal real mother wavelets for its computation. The HWT is associated with the bishrink filter. It processes the magnitudes of the HWT detail coefficients with directional windows for the estimation of the local standard deviation, σ. This association is sensitive to the selection of the mother wavelets used for the computation of the HWT. To reduce this sensitivity, we have conceived a two stage denoising method which acts in a multi-wavelet context. Our mother wavelets searching area was restricted to the Daubechies family. In the first stage, the input image is denoised using the association bishrink-HWT computed using Dau_6. The image of local variances of this first result represents the reference of the proposed denoising method. By the segmentation of the reference using the thresholds ε_k we generate the binary masks M_k. In the second stage is created the multi-wavelet context obtaining the partial results PR_k. Linear combination of those images are computed to correct the drawbacks of the bishrink filter obtaining the new partial results NPR_k. Different mother wavelets are associated with different regions of the useful component of the input image on the basis of the similarity of their space-frequency content with the aid of relation (26), obtaining the regions R_k. By their concatenation is obtained the final result. The advantage of the proposed multi wavelet approach can be observed comparing the results in table I with the results obtained applying the proposed denoising method presented on the sixth column of table II.

Acknowledgment

The research reported in this paper was developed in the framework of a grant of the Romanian Research Council (CNCSIS) with the title "Using Wavelets Theory for Decision Making" no. 349/13.01.09.

References

[1] D. L. Donoho, I. M. Johnstone, Ideal spatial adaptation by wavelet shrinkage, *Biometrika*, 81(3) : 425-455, 1994.

[2] N. Kingsbury, Complex Wavelets for Shift Invariant Analysis and Filtering of Signals, *Applied and Comp. Harm. Anal.* 10, 2001, 234-253.

[3] N G Kingsbury, A Dual-Tree Complex Wavelet Transform with improved orthogonality and symmetry properties, *Proc. IEEE Conf. on Image Processing*, Vancouver, September 11-13, 2000, paper 1429.

[4] I. Adam, C. Nafornita, J-M Boucher and A. Isar, "A New Implementation of the Hyperanalytic Wavelet Transform", Proc. of IEEE Sympo. *ISSCS 2007*, Iasi, Romania, 401-404.

[5] G.P. Nason, Choice of wavelet smoothness, primary resolution and threshold in wavelet shrinkage, *Statistics and Computing*, 12, 2002, 219-227.

[6] S. Mallat, A Wavelet Tour of Signal Processing, 2nd Edition, *Academic Press*, New York, 1999.

[7] Florian Luisier, Thierry Blu and Michael Unser, A New SURE Approach to Image Denoising: Interscale Orthonormal Wavelet Thresholding, *IEEE Transactions on Image Processing*, Vol. 16, No. 3, March 2007.

[8] Samuel Foucher, Gozie Bertin Benie, Jean-Marc Boucher, Multiscale MAP Filtering of SAR images, *IEEE Transactions on Image Processing*, vol. 10, no.1, January 2001, 49-60.

[9] L. Sendur and I. W. Selesnick, Bivariate shrinkage functions for wavelet-based denoising exploiting interscale dependency, *IEEE Trans. on Signal Processing*, 50(11): 2744-2756, November 2002.

[10] A. Achim and E. E. Kuruoglu, Image Denoising Using Bivariate α-Stable Distributions in the Complex Wavelet Domain, *IEEE Signal Processing Letters*, 12(1):17-20, January 2005.

[11] A. Pizurica, W. Philips, Estimating the probability of the presence of a signal of interest in multiresolution single and multiband image denoising, *IEEE Transactions on Image Process.* 15(3) (2006) 654-665.

[12] D. Gleich, M. Datcu, Gauss–Markov Model for Wavelet-Based SAR Image Despeckling, *IEEE Sig. Proc. Let.*, vol. 13, no. 6, June 2006, 365-368.

[13] C. Davenport, Commutative Hypercomplex Mathematics, http://home.usit.net/~cmdaven/cmdaven1.htm

[14] M. Oltean, A. Isar**,** On the Time-Frequency Localization of the Wavelet Signals with Application to Orthogonal Modulation, *Proceedings of IEEE International Symposium SCS'09*, Iasi, Romania, July 9-10, 2009, ISBN 1-4244-0968-3, pp. 173-176.

[15] I. Firoiu, C. Nafornita, J.-M. Boucher, A. Isar, Image Denoising Using a New Implementation of the Hyperanalytic Wavelet Transform, *IEEE*

Transactions on Instrumentation and Measurements, vol. 58, Issue 8, August 2009, pp. 2410-2416.
[16] P.-L. Shui, "Image Denoising Algorithm via Doubly Local Wiener Filtering With Directional Windows in Wavelet Domain", IEEE Sig. Proc. Let., Vol. 12, No. 6, '05, 681-684.
[17] Z.-F. Zhou and P.-L. Shui, Contourlet-based image denoising algorithm using directional windows, Elect. Let., vol 43, no.2, '07.
[18] S. C. Olhede, "Hyperanalytic Denoising", Imperial College Statistics Section Technical Report TR-06-01 1, Department of Mathematics, Imperial College London, SW7 2AZ UK.